# $Zr_{1-x}Ti_xSb$: A Novel Antimonide on the Quasibinary Section ZrSb−TiSb with a Complex Crystal Structure Exhibiting Linear Sb Chains and Fragments of the TiSb Structure

**Holger Kleinke**

*Contribution from the Department of Chemistry, University of Waterloo, Waterloo, Ontario, Canada N2L 3G1*

*Received September 20, 1999*

**Abstract:** $Zr_{1-x}Ti_xSb$ can be obtained in quantitative yields by arc-melting suitable mixtures of Zr, Ti, $ZrSb_2$, and $TiSb_2$, or alternatively via a solid-state reaction at 1200 °C. This phase, although situated on the quasibinary section ZrSb−TiSb, crystallizes in an unprecedented structure type with $0.38(3) \le x \le 0.549(6)$, which was determined by three single-crystal analyses using an IPDS diffractometer: space group *Cmcm*, $Z = 4$, lattice dimensions ranging from $a = 2455.8(2)$ pm, $b = 852.06(9)$ pm, $c = 566.69(5)$ pm ($x = 0.55$) to $a = 2479.7(6)$ pm, $b = 859.4(2)$ pm, $c = 568.91(9)$ pm ($x = 0.38$). The crystal structure consists in part of channels formed by the metal atoms (M = Zr, Ti), which include a planar Sb ladder exhibiting short Sb−Sb distances (284 pm = $c/2$) parallel and longer ones (ca. 347 pm) perpendicular to the chain directions. The channels are further surrounded by Sb atoms, which belong in part to the embedding NiAs-type fragments. In contrast to TiSb (NiAs type) and ZrSb (ZrSb type), the new structure is stabilized by *strong Sb−Sb bonding* (in addition to M−Sb and M−M bonding). This is supported by the results of band structure calculations based on the ab initio LMTO method as well as on the semiempirical extended Hückel approach, which both also suggest three-dimensional metallic properties. The metallic character is confirmed by measurements of the thermopower and the electrical resistivity.

## Introduction

Several different structure types occur among the valence-electron poor transition metal pnictides with a metal:pnicogen ratio of M:Pn = 1, including the types NaCl (representatives: MP, MAs, and MSb with M = Sc, Y),[1] NiAs ($VP$[2] and MSb with M = Ti, Nb),[3] MnP (VAs),[4] TiAs (MP and MAs with M = Ti, Zr, Hf),[5] NbP (NbP, NbAs, TaAs),[6] and ZrSb.[7] Apart from the NaCl type examples, all structures exhibit M−M bonding interactions in addition to the dominating M−Pn bonds. On the other hand, significant Pn−Pn bonding was observed only in the case of ZrSb, where Sb−Sb distances of ca. 324 pm occur. While these distances are much longer than typical Sb−Sb single bonds of 280−290 pm, a comparison with *bonding* closed-shell interactions such as in $Sb_2(CH_3)_4$ (distance $d_{Sb-Sb} = 368$ pm)[8] indicates significant orbital overlap in this case.

Since antimony is, apart from bismuth, the most electropositive Pn element considered here, it is understandable that Pn−Pn bonds occur only among the antimonides (the lack of examples with bismuth might stem from a lack of experimental effort), while the other Pn atoms are more likely to exhibit filled sp bands, inhibiting the formation of Pn−Pn contacts. However, with zirconium being more electropositive than titanium or niobium on any electronegativity scale, it remains unclear why Sb−Sb bonds are observed in ZrSb, but not in TiSb nor in NbSb.

Therefore, the pseudobinary section ZrSb−TiSb was investigated experimentally and theoretically, resulting in the discovery of $Zr_{1-x}Ti_xSb$ forming a novel structure type that is introduced in this article. The relations to ZrSb and TiSb are discussed, in particular with respect to the differences in bonding and the holes in the antimony centered sp bands.

The structure of the new phase $Zr_{1-x}Ti_xSb$ is of a new type, exhibiting differential fractional site occupancies on the metal positions, and it can be regarded as a typical DFSO-stabilized material, a concept developed by Franzen et al. (DFSO = differential fractional site occupancies).[9] While in most cases mixing related metal atoms just leads to the formation of solid solutions, mixed occupancy factors can favor structural complexity through diversity of metal atom sites. This is observed in phases prepared at rather high temperatures, i.e., when the configurational entropy plays a major role for the stability, and when distinct differences occur between the different metals used, such as between Ti and Hf[10] or between Zr and V,[11] or in

(1) ScP: *Inorg. Mater., Transl. Izvest. Akad. Nauk SSR, Neorg. Mater.* **1965**, *1*, 1361. ScAs, ScSb: Berger, R. *Acta Chem. Scand.* **1977**, *31A*, 514. YSb: Frick, B.; Schoenes, J.; Hulliger, F.; Vogt, O. *Solid State Commun.* **1984**, *49*, 1133.

(2) Fjellvåg, H.; Kjekshus, A. *Monatsh. Chem.* **1986**, *117*, 773.

(3) TiSb: Nowotny, H.; Peal, J. *Monatsh. Chem.* **1951**, *82*, 336. NbSb: Myzenkova, L. F.; Baron, V. V.; Savitsky, Y. M. *Russ. Metall., Transl. Izvest. Akad. Nauk SSR, Met.* **1966**, 89.

(4) Bachmayer, K.; Nowotny, H. *Monatsh. Chem.* **1955**, *86*, 741.

(5) TiP: Snell, P.-O. *Acta Chem. Scand.* **1967**, *21*, 1773. TiAs: Bachmayer, K.; Nowotny, H.; Kohl, A. *Monatsh. Chem.* **1955**, *86*, 39. ZrP: Bachmayer, K.; Nowotny, H.; Kohl, A. *Monatsh. Chem.* **1955**, *86*, 39. HfP: Jeitschko, W.; Nowotny, H. *Monatsh. Chem.* **1962**, *93*, 1107. HfAs: *Monatsh. Chem.* **1962**, *93*, 1284.

(6) NbP, NbAs, TaAs: Boller, H.; Parthé, E. *Acta Crystallogr.* **1963**, *16*, 1095. TaP: Willerström, J.-O. *J. Less-Common Met.* **1984**, *99*, 273.

(7) Garcia, E.; Corbett, J. D. *J. Solid State Chem.* **1988**, *73*, 452.

(8) Bürger, H.; Eujen, R.; Becker, G.; Mundt, O.; Westerhausen, M.; Witthauer, C. *J. Mol. Struct.* **1983**, *98*, 265.

(9) Yao, X.; Marking, G. A.; Franzen, H. F. *Ber. Bunsen-Ges. Phys. Chem.* **1992**, *96*, 1552. Franzen, H. F.; Köckerling, M. *Prog. Solid State Chem.* **1995**, *23*, 265. Kleinke, H.; Franzen, H. F. *J. Am. Chem. Soc.* **1997**, *119*, 12824.

10.1021/ja993423d CCC: $19.00 
Published on Web 01/20/2000

more metal-rich examples, where even minor differences between the metals (e.g, Nb/Ta)[12] become more important.

## Experimental Section

**Syntheses.** For the synthesis of (Zr,Ti)Sb, $TiSb_2$ and $ZrSb_2$ were prepared first in solid/liquid reactions of the elements titanium (ALFA, −100 mesh, 99.4%) and zirconium (ALFA, 4−20 mesh, purity 99.6%), respectively, and antimony (MERCK, powder, 99.8%, melting point 630 °C) in the stoichiometric 1:2 ratio at 650 °C in two evacuated fused silica tubes. In the next step, appropriate mixtures of $ZrSb_2$, $TiSb_2$, Zr, and Ti were pressed into pellets and then arc-melted once from each side on a water-cooled copper hearth under a flow of argon of 3 L/min. Since the observed weight loss of up to 5 wt % was identified by EDX investigations (see below) to stem from vaporized antimony, a slight excess of antimony (10%) in the form of $MSb_2$ (M = Zr, Ti) was added for compensation. Starting directly from the elements led to the same products, but with higher weight losses of 5−10 wt %. Since the subsequently successful structure determination showed the occurrence of different mixed Zr/Ti occupancies on some sites, solid-state reactions of the metals with the metal diantimonides, corresponding to the ideal stoichiometric ratios, were carried out in sealed tantalum tubes at 1200 °C over 96 h to investigate the influence of the reaction temperature on the different site occupancies.

**Phase Analyses.** No significant differences occurred between the powder diagrams obtained from samples prepared using different reaction conditions (i.e. arc-melting vs 1200 °C), indicating that the same structures formed. Reactions carried out at 1200 °C resulted in apparently homogeneous powder patterns in the cases of the initial compositions $Zr_{1-x}Ti_xSb$ with $0.4 \le x \le 0.55$, while the reflections were shifted toward smaller *d* values with increasing *x*, suggesting a noticeable phase range. ZrSb and $Zr_5Z_xSb_3$ (Z = Ti or Sb)[13] were identified as the main products in samples with higher Zr contents (i.e. $x < 0.4$), while the NiAs-type formed with varying lattice dimensions on the Ti-rich border (i.e. $x > 0.55$), suggesting an incorporation of zirconium in the TiSb structure.

To check for impurities, semiquantitative investigations of a sample of the starting composition $Zr_{0.5}Ti_{0.5}Sb$ were carried out using an electron microscope (CAMSCAN, CS 4DV) with an additional EDX device (detector: NORAN INSTRUMENTS). No impurities were found; the Zr:Ti:Sb ratio averaged over three crystals was determined to be 24(2):25(2):51(2).

**Structure Determinations.** Three crystals from different samples, namely one from each border of the phase range, prepared at 1200 °C, and one from an arc-melted sample with a nominal Zr:Ti ratio of 1, were measured on an IPDS diffractometer (STOE). The positions of up to 5000 reflections with $I > 6\sigma(I)$ were used to refine the lattice dimensions. The data were corrected for Lorentz and for Polarization effects. The space group *Cmcm* was chosen based on the systematic extinctions (*hkl*, $h + k = 2n$; *h*0*l*, $l = 2n$); lowering the symmetry by removing the inversion center (space group $Cmc2_1$) led to strong correlations between the sites which are equivalent in *Cmcm*, but to no improvement of the residual values.

The structure solution was performed with the data of the crystal of a sample with the nominal composition $Zr_{0.4}Ti_{0.6}Sb$ using the direct methods (SHELXS).[14] The four strongest peaks were attributed to Sb atoms, and the sites corresponding to the next strongest four peaks were assigned to be occupied by mixtures of the metal atoms Zr and Ti. The Zr contents were refined to different values in subsequent refinements (SHELXL),[15] namely 1.02(1) (M1), 0.71(1) (M2), 0.37(1) (M3), and 0.02(1) (M4), with the total occupancy factors of each site being restricted to be 100% ($f_{Zr} + f_{Ti} = 1$). Since the deviations from 1 and 0 were not significant in the cases of M1 and M4, these sites were considered to be occupied solely by zirconium (M1) and titanium (M4), respectively. With the multiplicity of the M1 and Sb1 sites being half of those of the other sites (4 vs 8), the chemical formula based on this information was refined to $Zr_{3.16(4)}Ti_{3.84}Sb_7$ with $Z = 4$ (i.e. $Zr_{1-x}Ti_xSb$ with $x = 0.549(6)$). The same procedure was used during the refinements of the other two data sets, yielding $Zr_{4.32(18)}Ti_{2.68}Sb_7$ ($x = 0.38(3)$) for the crystal of the Zr-rich sample and $Zr_{3.66(12)}Ti_{3.34}Sb_7$ ($x = 0.48(2)$) for the crystal of the arc-melted sample. Crystallographic details are summarized in Tables 1 and 2.

**Table 1.** Crystallographic Data for (Zr,Ti)Sb

| chemical formula | $Zr_{4.32(18)}Ti_{2.68}Sb_7$ | $Zr_{3.66(12)}Ti_{3.34}Sb_7$ | $Zr_{3.16(4)}Ti_{3.84}Sb_7$ |
|---|---|---|---|
| formula wt, g/mol | 1374.4 | 1346.8 | 1324.4 |
| temp, K | 295 | 295 | 295 |
| space group | *Cmcm* | *Cmcm* | *Cmcm* |
| *a*, pm | 2479.7(6) | 2465.8(2) | 2455.8(2) |
| *b*, pm | 859.4(2) | 854.31(8) | 852.06(9) |
| *c*, pm | 568.91(9) | 567.54(5) | 566.69(5) |
| *V*, $10^6$ pm$^3$ | 1212.4(4) | 1195.6(2) | 1185.8(2) |
| *Z* | 4 | 4 | 4 |
| calcd density, g cm$^{-3}$ | 7.53 | 7.48 | 7.42 |
| abs coeff, cm$^{-1}$ | 204.5 | 206.1 | 206.7 |
| $R(F)$,[a] $R_w(F^2)$[b] | 0.037, 0.068 | 0.029, 0.055 | 0.029, 0.058 |

[a] $R(F) = \sum||F_o| - |F_c||/\sum|F_o|$. [b] $R_w(F^2) = [\sum[w(F_o^2 - F_c^2)^2]/\sum[w(F_o^2)^2]\ ]^{1/2}$.

**Table 2.** Positional Parameters and Equivalent Displacement Parameters (M = Zr, Ti)

| atom | site | $x$[a] | $y$[a] | $z$[a] | $U_{eq}$/pm$^2$ [a] | $U_{eq}$/pm$^2$ [b] | $U_{eq}$/pm$^2$ [c] |
|---|---|---|---|---|---|---|---|
| Sb1 | 4c | 1/2 | 0.3885(3) | 1/4 | 78(6) | 82(2) | 87(2) |
| Sb2 | 8g | 0.11073(8) | 0.1129(2) | 1/4 | 79(5) | 90(2) | 91(2) |
| Sb3 | 8g | 0.27868(7) | 0.2002(2) | 1/4 | 83(5) | 86(2) | 93(2) |
| Sb4 | 8e | 0.42994(7) | 0 | 0 | 98(5) | 132(2) | 105(2) |
| M1 | 4c | 0 | 0.2439(5) | 1/4 | 69(9) | 73(3) | 75(3) |
| M2 | 8g | 0.1771(1) | 0.3881(3) | 1/4 | 88(11) | 87(5) | 91(5) |
| M3 | 8g | 0.3903(1) | 0.2683(3) | 1/4 | 66(13) | 73(5) | 68(6) |
| M4 | 8e | 0.2040(2) | 0 | 0 | 45(16) | 68(7) | 61(4) |

[a] $Zr_{4.3}Ti_{2.7}Sb_7$. [b] $Zr_{3.7}Ti_{3.3}Sb_7$. [c] $Zr_{3.2}Ti_{3.8}Sb_7$.

**Calculations of the Electronic Structure.** The structure parameters of the most Zr-rich compound, $Zr_{4.3}Ti_{2.7}Sb_7$, were taken for use in the calculations, since therein the assignments of the M atoms to the M sites are most straightforward: M1, M2, and M3 were treated as Zr (Zr occupancies experimentally determined: 100, 91(3), and 66(3)%, respectively) and M4 as Ti (Ti occupancy experimentally determined: 91(3)%), giving the hypothetical model structure $Zr_5Ti_2Sb_7$. The extended Hückel theory[16] was used to calculate the Mulliken gross and overlap populations[17] for the different interactions using a mesh of 140 *k* points of the reciprocal primitive unit cell. The Hückel parameters for Zr, Ti, and Sb were taken from standard sources,[18] and the ionization potentials of Zr and Ti were optimized by charge iteration on $Zr_2V_6Sb_9$[19] and TiSb,[20] respectively (Table 3).

Because the Hückel theory is known to depend strongly on the parameters used, LMTO calculations[21] were carried out to get more reliable results for the band structure and for detailed comparisons with ZrSb and TiSb. The integration in *k* space was performed by the

(10) $(Hf,Ti)_{21}S_8$: Harbrecht, B.; Franzen, H. F. *Z. Kristallogr.* **1989**, *186*, 119. $(Hf,Ti)_7Sb_4$: Kleinke, H. *Inorg. Chem.* **1999**, *38*, 2931.

(11) $(Zr,V)_{13}Sb_{10}$: Kleinke, H. *J. Chem. Soc., Chem. Commun.* **1998**, 2219. $(Zr,V)_{11}Sb_8$: Kleinke, H. *J. Mater. Chem.* **1999**, *9*, 2703.

(12) Yao, X.; Franzen, H. F. *J. Am. Chem. Soc.* **1991**, *113*, 1426. Yao, X.; Miller, G. J.; Franzen, H. F. *J. Alloys Compd.* **1992**, *183*, 7. Yao, X.; Franzen, H. F. *J. Solid State Chem.* **1990**, *86*, 88. Yao, X.; Franzen, H. F. *Z. Anorg. Allg. Chem.* **1991**, *589/599*, 353.

(13) $Zr_5Z_xSb_3$ (Z = Ti or Sb) was identified based on a Guinier diagram in analogy to $Zr_5ZSb_3$ with Z = Fe, Co, Ni, ..., see: Garcia, E.; Ku, H. C.; Shelton, R. N.; Corbett, J. D. *Solid State Commun.* **1988**, *65*, 757. The lattice dimensions as determined under the restriction of ideal hexagonal symmetry from a single crystal using the IPDS diffractometer are $a = 853.5(6)$ pm and $c = 583.9(4)$ pm.

(14) Sheldrick, G. M. *SHELXS-86*, University of Göttingen, Germany, 1986.

(15) Sheldrick, G. M. *SHELXL-97*, University of Göttingen, Germany, 1997.

(16) Hoffmann, R. *J. Chem. Phys.* **1963**, *39*, 1397. Whangbo, M.-H.; Hoffmann, R. *J. Am. Chem. Soc.* **1978**, *100*, 6093. Program EHMACC, adapted for use on a PC by M. Köckerling, Gesamthochschule Duisburg, 1997.

(17) Mulliken, R. S. *J. Chem. Phys.* **1955**, *23*, 2343.

(18) Clementi, E.; Roetti, C. *At. Nucl. Data Tables* **1974**, *14*, 177.

(19) Kleinke, H. *Eur. J. Inorg. Chem.* **1998**, 1369.

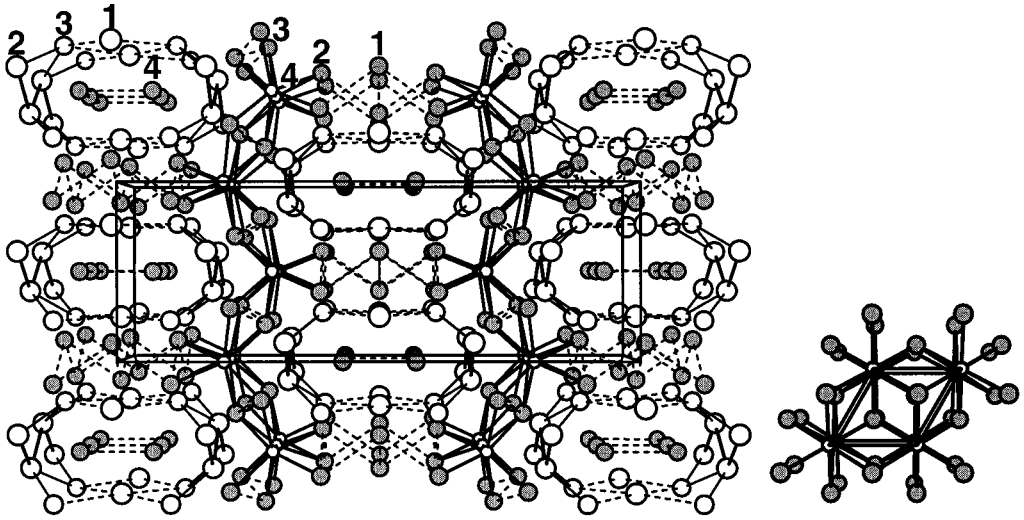


**Figure 1.** (Left) Projection of the structure of $Zr_{4.3}Ti_{2.7}Sb_7$ along [001], emphasizing the TiSb fragments and the $^1_\infty[M_{10}Sb_4]$ chains: horizontal, *a* axis; gray circles, Sb; white, Zr/Ti; the higher the Zr/Ti ratio, the larger the circles. Right: TiSb structure.

**Table 3.** Parameters Used for Extended Hückel Calculations

| orbital | $H_{ii}$/eV | $\varsigma 1$ | $c_1$ | $\varsigma_2$ | $c_2$ |
|---|---|---|---|---|---|
| Ti, 4s | −8.485 | 1.50 | | | |
| Ti, 4p | −4.603 | 1.50 | | | |
| Ti, 3d | −9.259 | 4.55 | 0.4391 | 1.600 | 0.7397 |
| Zr, 5s | −8.204 | 1.82 | | | |
| Zr, 5p | −4.593 | 1.78 | | | |
| Zr, 4d | −8.117 | 3.84 | 0.6213 | 1.510 | 0.5798 |
| Sb, 5s | −18.80 | 2.32 | | | |
| Sb, 5p | −11.70 | 2.00 | | | |

tetrahedron method[22] on a grid of 1221 irreducible *k* points of the first Brillouin zone. The electronic structures of ZrSb and TiSb were also calculated with both methods, extended Hückel and LMTO.

**Physical Property Measurements.** The properties of a sample of the nominal composition $Zr_{4.2}Ti_{2.8}Sb_7$ (i.e. $Zr_{1-x}Ti_xSb$ with $x = 0.4$) were determined. Temperature-dependent resistivity measurements down to 10 K were performed on a cold-pressed bar of the dimensions of 0.2 cm × 0.1 cm × 0.15 cm applying a four-contact method. Absolute Seebeck coefficients were determined on the same cold-pressed bar at six different temperature gradients to check for consistency.

## Results and Discussion

**Crystal Structures.** $Zr_{1-x}Ti_xSb$ with $0.38(3) \le x \le 0.549(6)$ occurs in a new structure type, which is shown in Figure 1. The structure exhibits two distinct structural motifs, namely (distorted) fragments of the TiSb structure (NiAs type), i.e., chains of face-condensed $MSb_6$ octahedra (left part of Figure 2) interconnected to puckered layers via common edges, on one hand, and on the other hand linear infinite channels formed by M1−3, each of which includes two parallel chains of Sb4. The buckled layers consisting of the $MSb_6$ octahedra are separated by the Sb1 atoms and the $^1_\infty[M_{10}Sb_4]$ chains (middle of Figure 2). While two of these layers occur within one unit cell, being related to another by an inversion center and thus staggered

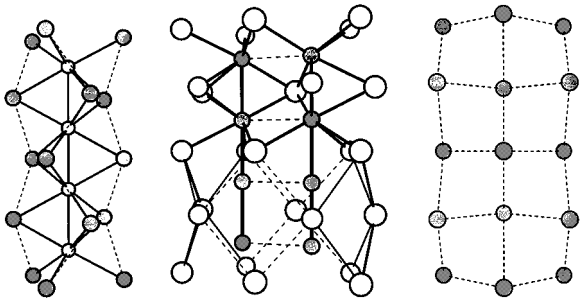

**Figure 2.** Sections of the columnar structure motifs; vertical, *c* axis: (left) face-condensed $M4Sb_6$ octahedra; (middle) the $^1_\infty[M_{10}Sb_4]$ chain; (right) section of a $4^4$ net of Sb atoms.

with respect to each other, topologically equivalent layers being in register by translational symmetry were found in the structure of $LnCrSb_3$ (with Ln = La, Ce, Pr, Nd, Sm, Tb, Dy).[23]

The $^1_\infty[M_{10}Sb_4]$ chains are embedded between Sb atoms, which belong in part to the TiSb-like fragments. The metal site of the TiSb fragments (M4) shows a maximum incorporation of only 9% zirconium, i.e., it consists primarily of titanium, even at the Zr-rich border. A view down the crystallographic *c* axis is given in Figure 1, emphasizing the NiAs-like fragments and the $^1_\infty[M_{10}Sb_4]$ chains, with the inset showing a projection of the structure of TiSb for comparison.

(Zr,Ti)Sb can be considered as the Sb-richest member of a recently discovered family of ternary antimonides, which consists to date of $(Zr,V)_{13}Sb_{10}$, $(Zr,V)_{11}Sb_8$,[11] and $Ti_{11}Sb_8$.[24] The common structural features are the same kind of NiAs-like fragments, with metal sites which are in every case predominately occupied by the 3d metal atoms Ti and V, respectively, and channels including linear chains of Sb atoms with interatomic distances <290 pm. The linear Sb chains are pairwise interconnected to form Sb ladders via Sb−Sb distances of ca. 347 pm only in the case of (Zr,Ti)Sb. Furthermore, the metal polyhedra surrounding the Sb atoms of the linear chain are face-condensed defect $M_7\square_1$ square antiprisms (□ = vacancy) in the structures of $(Zr,V)_{13}Sb_{10}$, $(Zr,V)_{11}Sb_8$, and $Ti_{11}Sb_8$, but face-condensed $M_6$ octahedra which are interconnected by common edges to double chains in the case of (Zr,Ti)Sb.

(20) To verify that TiSb exists with the exact Ti:Sb ratio of 1:1 and not (only) as a self-intercalated $Ti_{1+x}Sb$, its crystal structure was redetermined from single-crystal data for the first time. The NiAs structure type was confirmed: space group $P6_3/mmc$, $a = 401.35(7)$ pm, $c = 629.9(1)$ pm, Ti on (0, 0, 0), $U_{eq} = 113(32)$ pm$^2$; Sb on (1/3, 2/3, 1/4), $U_{eq} = 114(11)$ pm$^2$; $R_w(F_o^2) = 0.082$, $\Delta\rho_{max} = 2.2$ e Å$^{-3}$.

(21) van Barth, U.; Hedin, L. *J. Phys.* **1971**, *C4*, 2064. Andersen, O. K. *Phys. Rev.* **1975**, *B12*, 3060. Skriver, H. L. *The LMTO Method*; Springer: Berlin, 1984.

(22) Jepsen, O.; Andersen, O. K. *Solid State Commun.* **1971**, 9.

(23) Brylak, M.; Jeitschko, W. *Z. Naturforsch. B: Chem. Sci.* **1995**, *50*, 899. Ferguson, M. J.; Hushagen, R. W.; Mar, A. *J. Alloys Compd.* **1997**, *249*, 191.

(24) Kleinke, H. *Z. Kristallogr.* **1999**, *Suppl. 16*, 42.

While the structure of (Zr,Ti)Sb is partially reminiscent of the TiSb structure, no obvious structural relations exist between the new phase and the structure of ZrSb. The latter contains the Zr atoms in mono-capped trigonal $ZrSb_7$ prisms and in trigonal $ZrSb_5$ bipyramids, and puckered hexagonal Sb layers which resemble the layers in the structure of elemental antimony.[7] Here, the Sb atoms form ladders in the $^1_\infty[M_{10}Sb_4]$ chains, zigzag chains in the TiSb-like fragments, and sections of puckered $4^4$ nets (right part of Figure 2), which alternate with the $^1_\infty[M_{10}Sb_4]$ chains parallel to [010]. Furthermore, the coordination polyhedra of the M atoms, which can be described as distorted mono-capped square $M1Sb_9$ antiprisms, pentagonal $M2Sb_7$ and $M3Sb_7$ bipyramids, and $M4Sb_6$ octahedra, are different. Note that among these three topologically different coordination spheres, only the mono-capped square antiprisms are not observed in the structures of $(Zr,V)_{13}Sb_{10}$, $(Zr,V)_{11}Sb_8$, and $Ti_{11}Sb_8$, because the Sb ladder forms one "square" of those polyhedra, while the pentagonal bipyramids and the octahedra occur in these structures, also. The capped square antiprismatic Sb coordination is familiar from rare earth antimonides (e.g., $LnSb_2$[25] and $LnCrSb_3$[23]), albeit not found yet in Zr antimonides, possibly due to the smaller size of Zr compared to the rare earth elements.

Despite the reminiscence of the TiSb structure in (Zr,Ti)Sb, the Sb substructure of (Zr,Ti)Sb is more, though not strongly, related to ZrSb than to TiSb, because the shortest Sb−Sb distances are 324 and 325 pm in ZrSb and 391 pm in TiSb. In the structure of $Zr_{4.3}Ti_{2.7}Sb_7$, the variety of Sb−Sb distances includes a short one of 284 pm and intermediate distances varying from 329 to 348 pm, while all of these distances are slightly shorter in the more Ti-rich examples, $Zr_{3.7}Ti_{3.3}Sb_7$ and $Zr_{3.2}Ti_{3.8}Sb_7$ (Table 4). The distance of 284 pm is shorter than the shortest bonds in elemental antimony (291 pm) and typical for single bonds, which occur in the structures of KSb (283 and 285 pm),[26] *cyclo*-$Sb_5^{5-}$ (between 281 and 291 pm),[27] and $Sb_{11}^{3-}$ (between 276 and 285 pm).[28] The other distances may be compared to (bonding) van der Waals interactions such as the one in $Sb_2(CH_3)_4$ (368 pm)[8] or to the interlayer distance of 335 pm in elemental antimony, the three-dimensional mechanical properties of which suggest modest, but significantly positive overlap between the layers. The character of the Sb−Sb interactions in (Zr,Ti)Sb, ZrSb, and TiSb will be discussed in detail in the chapter dealing with the electronic structure. The fact, however, that the Sb4 atoms are shifted toward each other out of the basal plane of the $M_6$ octahedra indicates bonding Sb−Sb interactions between two neighboring Sb4 chains, i.e., along the steps of the Sb ladders with $d_{Sb-Sb} = 347$ pm.

Besides the homoatomic Sb−Sb interactions, M−M interactions occur in all three examples of structures with a metal: antimony ratio of 1:1 discussed here. Even if a complete electron transfer from the M atoms to the Sb atoms occurred, corresponding to the ionic formulation $M^{3+}Sb^{3-}$, one electron per M atom would still be available for the formation of M−M bonds. The shortest M−M distances occur in the TiSb-like fragments of (Zr,Ti)Sb, namely 284 pm = $c/2$ in the linear M4 chain parallel to the $c$ axis. While the corresponding distance in TiSb (315 pm) is significantly larger, the shortest Zr−Zr distances in ZrSb are even longer, namely 339 and 340 pm. This correlates well with the difference in the Pauling single bond radii of titanium (132 pm) and zirconium (145 pm).[29] Using Pauling's equation $d(n) = d(1) - 60$ pm $\times \log n$ (with $n$ = bond order), the Pauling bond orders (PBO) are calculated to 0.46 for the Ti−Ti bond in (Zr,Ti)Sb and 0.14 and 0.15 for the shortest M−M bonds in TiSb and ZrSb, respectively. The shortest M−M contacts with M2 and M3 in (Zr,Ti)Sb range from 336 to 342 pm, thus being comparable to those in ZrSb, despite significant Ti contents between 37 and 91%. M1 stands out, being the only atom without any M−M distance shorter than 390 pm.

However, the heteroatomic M−Sb bonds predominate by number and shortness in all three structures considered, being

**Table 4.** Selected Interactions in the Structures of (Zr,Ti)Sb

| bond | | MOP[a] | distance/pm[b] | distance/pm[c] | distance/pm[d] |
|---|---|---|---|---|---|
| Sb1−M3 | 2× | 0.462 | 291.0(3) | 288.1(2) | 287.1(2) |
| Sb1−M1 | 1× | 0.354 | 305.4(5) | 305.0(2) | 304.9(2) |
| Sb1−M1 | 2× | 0.343 | 306.4(2) | 305.28(8) | 304.60(8) |
| Sb1−Sb2 | 2× | 0.031 | 335.5(2) | 334.3(1) | 333.0(1) |
| Sb1−Sb1 | 2× | 0.043 | 343.0(2) | 342.87(1) | 342.87(9) |
| Sb2−M2 | 1× | 0.424 | 288.1(3) | 287.1(2) | 286.6(2) |
| Sb2−M4 | 2× | 0.288 | 288.3(3) | 285.8(2) | 284.9(2) |
| Sb2−M3 | 1× | 0.318 | 296.2(3) | 293.4(2) | 291.7(2) |
| Sb2−M1 | 1× | 0.354 | 296.8(3) | 295.8(1) | 295.3(1) |
| Sb2−M3 | 2× | 0.300 | 302.2(1) | 301.33(7) | 301.22(7) |
| Sb2−Sb1 | 1× | 0.031 | 335.5(2) | 334.3(1) | 333.0(1) |
| Sb2−Sb2 | 2× | 0.035 | 344.3(1) | 342.68(7) | 340.88(6) |
| Sb2−Sb4 | 2× | −0.014 | 375.6(2) | 373.99(9) | 373.63(8) |
| Sb3−M3 | 1× | 0.426 | 282.8(4) | 281.3(2) | 279.2(2) |
| Sb3−M2 | 1× | 0.371 | 289.8(3) | 287.1(2) | 286.5(2) |
| Sb3−M4 | 2× | 0.278 | 290.0(3) | 289.6(1) | 288.7(1) |
| Sb3−M4 | 2× | 0.226 | 297.4(2) | 296.01(8) | 295.22(8) |
| Sb3−M2 | 1× | 0.261 | 299.2(3) | 297.9(2) | 296.5(2) |
| Sb3−M2 | 2× | 0.206 | 314.2(1) | 312.65(8) | 311.44(7) |
| Sb3−Sb3 | 2× | 0.069 | 329.4(1) | 329.18(7) | 329.12(6) |
| Sb4−Sb4 | 2× | 0.375 | 284.45(5) | 283.77(3) | 283.35(3) |
| Sb4−M3 | 2× | 0.366 | 288.2(2) | 286.9(2) | 285.7(2) |
| Sb4−M1 | 2× | 0.238 | 314.4(3) | 312.6(1) | 312.5(1) |
| Sb4−M2 | 2× | 0.191 | 316.1(3) | 315.0(2) | 313.4(1) |
| Sb4−Sb4 | 1× | 0.062 | 347.5(3) | 345.8(1) | 347.3(1) |
| Sb4−Sb2 | 2× | −0.014 | 375.6(2) | 373.99(9) | 373.63(8) |
| M1−Sb2 | 2× | 0.354 | 296.8(3) | 295.8(1) | 295.3(1) |
| M1−Sb1 | 1× | 0.354 | 305.4(5) | 305.0(2) | 304.9(2) |
| M1−Sb1 | 2× | 0.343 | 306.4(2) | 305.28(8) | 304.60(8) |
| M1−Sb4 | 4× | 0.238 | 314.4(3) | 312.6(1) | 312.5(1) |
| M1−M3 | 4× | 0.050 | 393.8(2) | 391.7(1) | 390.9(1) |
| M2−Sb2 | 1× | 0.424 | 288.1(3) | 287.1(2) | 286.6(2) |
| M2−Sb3 | 1× | 0.377 | 289.8(3) | 287.1(2) | 286.5(2) |
| M2−Sb3 | 1× | 0.261 | 299.2(3) | 297.9(2) | 296.5(2) |
| M2−Sb3 | 2× | 0.206 | 314.2(1) | 312.65(8) | 311.44(7) |
| M2−Sb4 | 2× | 0.191 | 316.1(3) | 315.0(2) | 313.4(1) |
| M2−M4 | 2× | 0.104 | 341.2(4) | 339.5(2) | 337.5(2) |
| M2−M2 | 2× | 0.114 | 343.4(2) | 342.0(1) | 342.2(1) |
| M2−M3 | 2× | 0.082 | 356.2(2) | 355.9(1) | 354.9(1) |
| M2−M3 | 1× | 0.055 | 367.0(4) | 365.9(2) | 365.5(2) |
| M2−M4 | 2× | 0.039 | 368.7(3) | 366.6(2) | 365.0(2) |
| M3−Sb3 | 1× | 0.426 | 282.8(4) | 281.3(2) | 279.2(2) |
| M3−Sb4 | 2× | 0.366 | 288.2(2) | 286.9(2) | 285.7(2) |
| M3−Sb1 | 1× | 0.462 | 291.0(3) | 288.1(2) | 287.1(2) |
| M3−Sb2 | 1× | 0.318 | 296.2(3) | 293.4(2) | 291.7(2) |
| M3−Sb2 | 2× | 0.300 | 302.2(1) | 301.33(7) | 301.22(7) |
| M3−M4 | 2× | 0.084 | 338.4(4) | 336.3(2) | 335.6(2) |
| M3−M2 | 2× | 0.082 | 356.2(2) | 355.9(1) | 354.9(1) |
| M3−M2 | 1× | 0.055 | 367.0(4) | 365.9(2) | 365.5(2) |
| M3−M4 | 2× | 0.050 | 393.8(2) | 391.7(1) | 390.9(1) |
| M4−M4 | 2× | 0.268 | 284.45(5) | 283.77(3) | 283.35(3) |
| M4−Sb2 | 2× | 0.288 | 288.3(3) | 285.8(2) | 284.9(2) |
| M4−Sb3 | 2× | 0.278 | 290.0(3) | 289.6(1) | 288.7(1) |
| M4−Sb3 | 2× | 0.226 | 297.4(2) | 296.01(8) | 295.22(8) |
| M4−M3 | 2× | 0.084 | 338.4(4) | 336.3(2) | 335.6(2) |
| M4−M2 | 2× | 0.104 | 341.2(4) | 339.5(2) | 337.5(2) |
| M4−M2 | 2× | 0.039 | 368.7(3) | 366.6(2) | 365.0(2) |

[a] Values obtained from an Extended Hückel calculation on the structure model $Zr_5Ti_2Sb_7$. [b] $Zr_{4.3}Ti_{2.7}Sb_7$. [c] $Zr_{3.7}Ti_{3.3}Sb_7$. [d] $Zr_{3.2}Ti_{3.8}Sb_7$.

(25) Wang, R.; Steinfink, H. *Inorg. Chem.* **1967**, *6*, 1685. Eatough, N. L.; Hall, H. T. *Inorg. Chem.* **1969**, *8*, 1439.
(26) Hönle, W.; von Schnering, H.-G. *Z. Kristallogr.* **1981**, *155*, 307.
(27) Korber, N.; Richter, F. *Angew. Chem., Int. Ed. Engl.* **1997**, *36*, 1512.
(28) Bolle, U.; Tremel, W. *J. Chem. Soc., Chem. Commun.* **1992**, 91.
(29) Pauling, L. *The Nature of the Chemical Bond*, 3rd ed.; Cornell University Press: Ithaca, NY, 1948.

**Table 5.** Site Occupancies[a] and Pauling Bond Orders for (Zr,Ti)Sb

| | M1 | M2 | M3 | M4 |
|---|---|---|---|---|
| $f_{Zr}$[b] | 1 | 0.91(3) | 0.66(3) | 0.09(3) |
| $\sum PBO^b(r_M = r_{Zr})$ | 2.98 | 4.03 | 4.60 | 6.72 |
| $\sum PBO^b(r_M = r_{Ti})$ | 2.28 | 2.75 | 3.31 | 3.89 |
| $f_{Zr}$[c] | 1 | 0.71(2) | 0.52(2) | 0.10(2) |
| $\sum PBO^c(r_M = r_{Zr})$ | 3.94 | 5.15 | 6.03 | 8.02 |
| $\sum PBO^c(r_M = r_{Ti})$ | 2.39 | 2.91 | 3.53 | 4.09 |
| $f_{Zr}$[d] | 1 | 0.71(1) | 0.37(1) | 0 |
| $\sum PBO^d(r_M = r_{Zr})$ | 3.99 | 5.35 | 6.31 | 8.27 |
| $\sum PBO^d(r_M = r_{Ti})$ | 2.42 | 3.03 | 3.70 | 4.22 |

[a] $f_{Zr} + f_{Ti} = 1$. [b] $Zr_{4.3}Ti_{2.7}Sb_7$. [c] $Zr_{3.7}Ti_{3.3}Sb_7$. [d] $Zr_{3.2}Ti_{3.8}Sb_7$.

only slightly larger than the sums of the atom radii ($r_{Sb} = 139$ pm; $r_{Ti} + r_{Sb} = 271$ pm; $r_{Zr} + r_{Sb} = 284$ pm). The shortest occur in TiSb (280 pm) and in the TiSb-like fragment of (Zr,Ti)Sb (285−297 pm), while the structure of ZrSb exhibits Zr−Sb bonds ranging from 291 to 311 pm. The latter are comparable to the M1−Sb bonds in (Zr,Ti)Sb (295−314 pm), with M1 occupied solely by zirconium over the whole experimentally detected phase range. The M2−Sb and M3−Sb bonds are intermediate, varying from 287 to 316 pm and 279 to 302 pm, respectively.

**Site Preferences.** While (Zr,Ti)Sb is the first known DFSO-stabilized material with M = Zr and Ti, two examples were reported with Hf instead of Zr, e.g., $(Hf,Ti)_{21}S_8$ and $(Hf,Ti)_7Sb_4$.[10] In the latter two cases, it is difficult to detect any tendencies concerning the different site occupancies because opposed trends compete, based on the differences in size, electronegativity, and tendency to form metal−metal bonding. On the other hand, straightforward explanations were given for the experimentally observed site preferences in ternary niobium tantalum sulfides, where the Nb:Ta ratio decreases from one site to another with increasing metal−metal bonding per site,[12] and in the ternary zirconium vanadium antimonides $(Zr,V)_{13}Sb_{10}$ and $(Zr,V)_{11}Sb_8$, where the Zr:V ratio increases with increasing M−Sb distances.[11]

From all the DFSO examples known to date, (Zr,Ti)Sb is the least transition-metal-rich one. It is proposed that the differences in the predominating M−Sb interactions readily explain the different site preferences. Since titanium and zirconium are in the same group of the periodic table, they are isovalent and comparable in their electronegativity, compared to antimony. Thus, one can concentrate in a first approximation on the differences in size. Ti atoms, being smaller than Zr atoms, should prefer the sites with fewer Sb neighbors and shorter M−Sb contacts. To test this suggestion, the sums of the M−Sb Pauling bond orders (PBOs) were calculated twice for each M site using the radius of Ti as well as the radius of Zr (Table 5), because the bond lengths as well as the number of the bonds are reflected in these calculated values. As depicted in Figure 3, the Zr content increases from site to site with decreasing PBOs in all three structures, $Zr_{4.3}Ti_{2.7}Sb_7$, $Zr_{3.7}Ti_{3.3}Sb_7$, and $Zr_{3.2}Ti_{3.8}Sb_7$, independent of the metal atom radius used. This confirms the trend expected.

The configurational entropy favors complete disorder on all sites, but the difference in the enthalpy, $\delta H$, leads to partial ordering, namely different Zr:Ti ratios on the different sites. That these two effects compete is reflected in different ordering in samples prepared at different temperatures, because the importance of the entropy contribution $\delta S$ to the free enthalpy $\delta G = \delta H - T\delta S$ increases with increasing temperature $T$. Although direct comparisons of the three structures investigated here are inhibited by significant differences in composition, one can notice that the disorder is more pronounced in the phase prepared from the melt ($Zr_{3.7}Ti_{3.3}Sb_7$) than in the phases obtained via solid-state reactions ($Zr_{4.3}Ti_{2.7}Sb_7$ and $Zr_{3.2}Ti_{3.8}Sb_7$): the differences in the site occupancies between M2 and M4 are smallest in the case of the arc-melted $Zr_{3.7}Ti_{3.3}Sb_7$ ($\Delta f_{Zr} = 0.71 - 0.10 = 0.61$; $Zr_{4.3}Ti_{2.7}Sb_7$, 0.82; $Zr_{3.2}Ti_{3.8}Sb_7$, 0.71; M1 is always occupied by 100% Zr), i.e., the configurational entropy is largest. This is not a consequence of the different composition, because the arc-melted compound is intermediate in the Zr:Ti ratio, but shows the lowest Zr content on M2 and the highest on M4.

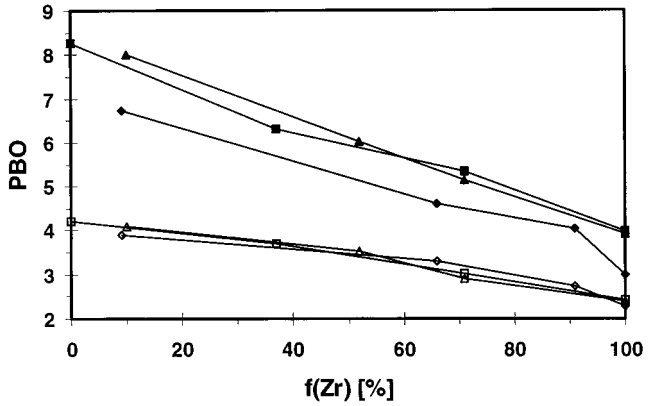


**Figure 3.** Pauling bond orders (PBO) vs Zr occupancies f(Zr): diamonds, $Zr_{4.3}Ti_{2.7}Sb_7$; triangles, $Zr_{3.7}Ti_{3.3}Sb_7$; squares, $Zr_{3.2}Ti_{3.8}Sb_7$; open symbols, $r_M = r_{Ti}$; black, $r_M = r_{Zr}$.

**Electronic Structures.** The band structure of the structure model $Zr_5Ti_2Sb_7$, as obtained from calculations using the LMTO approach, is shown along selected directions labeled according to Bradley and Cracknell[30] in Figure 4. The metal-centered bands are depicted via the *fat band* representation.[31] Several bands with mainly Zr d character cross the Fermi level, e.g., parallel (Γ−Z, T−Y, S−R) and perpendicular (T−Y, Y−Γ) to *c**, the direction of the Sb4 chain, strongly suggesting three-dimensional metallic properties. The Ti d bands occur in the same area, with the striking (filled) fat band with $d_{z^2}$ character around 1 eV below the Fermi level. The Ti−Ti bonding parallel to [001] is reflected in this band.

The projections of the band structures of ZrSb (left part in Figure 5) and TiSb (right part in Figure 5) also show as a common feature metal centered states predominating at the Fermi level. The p block of antimony is basically located between 1 and 5 eV below the Fermi level in the case of TiSb, while due to the Sb−Sb interactions, it is much broader in ZrSb. However, a tail of the Sb peak goes up above the Fermi edge in both cases, indicating the existence of holes in the sp band of antimony in ZrSb as well as in TiSb. It is concluded that the absence of Sb−Sb bonding in TiSb is not due to a (hypothetical) complete reduction of Sb. Correspondingly, the Mulliken charge (calculated with the extended Hückel approximation) of the Sb atom in TiSb is less negative (−0.36) than the average charge of the Sb atoms in ZrSb (−0.42). In the latter case, the Sb atom which takes part in the Sb−Sb bonding has a less negative charge (−0.33) than the one that does not (−0.61).

On a side note: since the sp holes are used to form Sb−Sb bonds in ZrSb only, TiSb is a candidate for a reduction with metals such as lithium or copper, which might result in filling the holes in the sp band. Rouxel published an overview of the possibilities of using the sp holes with respect to the so-called *chimie douce* (soft chemistry).[32]

(30) Bradley, C. J.; Cracknell, A. P. *The Mathematical Theory of Symmetry in Solids*; Clarendon Press: Oxford, 1972.
(31) Jepsen, O.; Andersen, O. K. *Z. Phys.* **1995**, *97*, 25.
(32) Rouxel, J. *Chem. Eur. J.* **1996**, *2*, 1053.

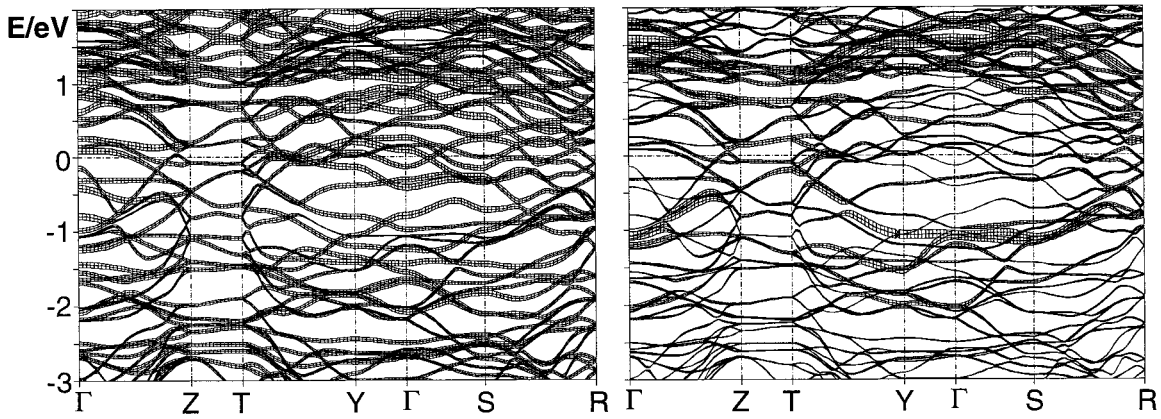


**Figure 4.** Band structure of $Zr_5Ti_2Sb_7$: dashed horizontal line at 0 eV shows the Fermi level. The bands with M orbital character (left: Zr, i.e., M1−3; right: Ti (M4)) are emphasized via the *fat band* representation.

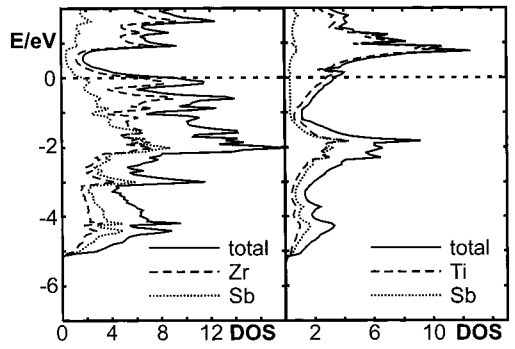


**Figure 5.** Densities of states for ZrSb (left) and TiSb (right). Dashed horizontal line at 0 eV shows the Fermi level.

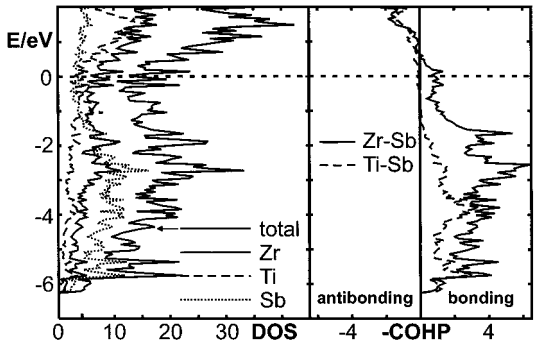


**Figure 6.** Densities of states (left) and selected COHP curves (M−Sb, right) for $Zr_5Ti_2Sb_7$. Dashed horizontal line at 0 eV shows the Fermi level.

The densities of states of the structure model $Zr_5Ti_2Sb_7$ are shown in the left part of Figure 6. The p states of antimony dominate the region below 2 eV below the Fermi level, while Zr and Ti contributions at these energies indicate the covalency of the M−Sb interactions. As mentioned above, the M-centered states predominate around the Fermi level, but significant densities of states at the Fermi level are deduced to arise from Sb states, also. The presence of holes in the sp band of antimony was expected based on the observation of some Sb−Sb contacts shorter than in elemental antimony. The increased importance of Sb−Sb bonding, compared to ZrSb and TiSb, is reflected in a less negative average Mulliken charge of the Sb atoms of −0.23. Furthermore, the charge of the Sb4 atom, which forms the linear chain with short interatomic distances of 284 pm, stands out with −0.01; the average charge of the other three Sb atoms in (Zr,Ti)Sb (−0.32) resembles the charge of the Sb atom in ZrSb (−0.33), which forms Sb−Sb bonds with distances in the range 324−325 pm.

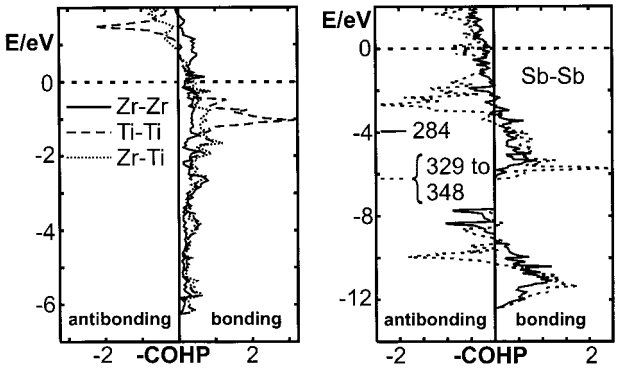


**Figure 7.** Selected COHP curves (left, M−M; right, Sb−Sb) for $Zr_5Ti_2Sb_7$. Dashed horizontal lines at 0 eV show the Fermi levels.

The M−Sb crystal orbital Hamiltonian populations,[33] cumulated over all M−Sb distances shorter than 320 pm per primitive unit cell, show that only bonding M−Sb states are filled (right part of Figure 6). The Ti−Sb interactions are roughly optimized, whereas some bonding Zr−Sb states remain empty. The latter is true also for the three different kinds of M−M interactions, namely Zr−Zr, Ti−Ti, and Zr−Ti (left part of Figure 7), all showing significant bonding overlap. The Ti-centered peak at −1 eV stems from the bonding $d_{z^2}-d_{z^2}$ interaction, i.e., the bond of 284 pm parallel to [001]. Altogether, the contribution of the M−M bonding to the stability of (Zr,Ti)Sb is apparently smaller than that of the M−Sb bonds, but still significant.

The only filled antibonding states in the structure of (Zr,Ti)-Sb occur in the Sb−Sb interactions (right part of Figure 7), which become antibonding already 3 eV below the Fermi level. However, very significantly positive net overlap results for the short bond (284 pm) by integrating over all states up to the Fermi level, since the bonding states outweigh the antibonding by far, and the longer contacts have only small, but positive overlap populations.

For detailed comparisons, we refer to the Mulliken overlap populations (MOP) obtained from extended Hückel calculations, which serve as a tool for the evaluation of relative bond strengths. MOPs of typical single bonds are of the order of 0.65 electrons per bond, as calculated for the bonds in KSb, and the values for the interactions in elemental antimony are 0.53 (291 pm) and 0.08 (335 pm), respectively.[34] Values similar to the latter are calculated for the Sb−Sb interactions in ZrSb (324 pm, 0.06; 325 pm, 0.09) and for the distances in (Zr,Ti)Sb between 329 and 348 pm (0.07−0.03), indicating weak bonding

(33) Dronskowski, R.; Blöchl, P. *J. Phys. Chem.* **1993**, *97*, 8617.
(34) Kleinke, H. Unpublished calculations, **1997**.

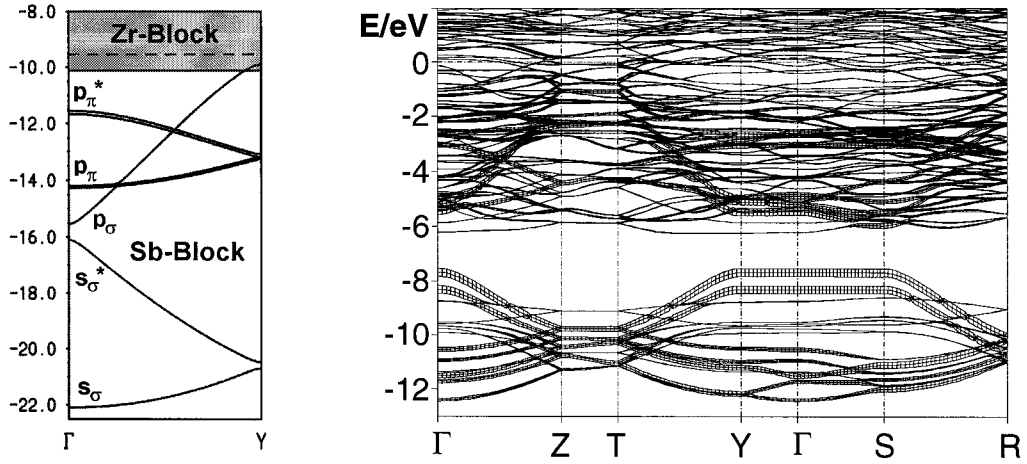


**Figure 8.** (Left) Schematic extended Hückel model of a $^1_\infty[Zr_7Sb_2]$ chain. (Right) Band structure of $Zr_5Ti_2Sb_7$. The bands with Sb4 orbital character are emphasized via the *fat band* representation. Dashed horizontal lines show the Fermi levels.

interactions in every case. Comparable values were also found for the interactions between 328 and 350 pm in the structures of $(Zr,V)_{11}Sb_8$ (averaged 0.02),[11] $Zr_2V_6Sb_9$ (0.04),[19] $(Hf,Ti)_7Sb_4$ (0.04),[10] and $Zr_3Ni_3Sb_4$ (0.03).[35] The small positive values suggest weak bonding character, which was also obtained using quasirelativistic pseudopotential ab initio calculations at the second-order Moller−Plesset level (MP2) for even longer distances; also an Sb−Sb attraction was calculated for the Sb−Sb interaction of 378.5 pm in the dipnicogen hydride model dimer $(H_2Sb-SbH_2)_2$ due to correlation effects.[36] These theoretical results are supported by measurements of the force constant (0.125 N cm$^{-1}$) of the intermolecular Sb−Sb interaction (368 pm) in $[(CH_3)_2Sb-Sb(CH_3)_2]_2$, which is more than 10% of the value for the intramolecular single bond of 284 pm (1.1 N cm$^{-1}$).[8] On the other hand, negative overlap populations were calculated for all Sb−Sb distances larger than 375 pm, including −0.014 ($d_{Sb2-Sb4}$ = 376 pm) in (Zr,Ti)Sb, −0.017 and −0.019 for the Sb−Sb bonds parallel to [100] in ZrSb (383 pm), and −0.002 (391 pm) and −0.004 (401 pm) in TiSb, while no intermediate distance, i.e., between 350 and 375 pm, occurs in any of these structures.

However, the Sb−Sb bond of 284 pm in the *linear* Sb4 chain of the structure of (Zr,Ti)Sb cannot be considered as a single bond, despite its short length, because that would require an $sp^3$ hybridization and thus the formation of a zigzag chain, as found for example in elemental tellurium. It was shown for the linear Sb chain with alternating interatomic distances of 280 and 288 pm in the structure of $(Zr,V)_{13}Sb_{10}$ that the bonds are described best as delocalized one-electron-two-center $\sigma$ bonds, via extended Hückel calculations of the model $^1_\infty[Zr_7Sb_2]$.[11] This is depicted in the left part of Figure 8: the $s_\sigma$, $s_\sigma^*$, $p_\pi$, $p_\pi^*$, and $p_\sigma$ bands of the two Sb atoms are situated well below the Fermi level, with the $p_\pi$ bands being formed from both the $p_x$ and the $p_z$ orbitals ($p_y$ is in this case parallel to the chain direction). Since only the $p_\sigma^*$ band remains empty, the Sb atoms are considered to be Sb(−II), each forming two Sb−Sb bonds with a bond order of $^1/_2$. The LMTO calculations reveal this model being in principle valid in the case of the Sb4 substructure of (Zr,Ti)Sb, also. The band structure of the structure model $Zr_5Ti_2Sb_7$ is reminiscent of the Sb bands discussed above, which can be taken from a comparison of the extended Hückel model with the bands exhibiting Sb4 character in (Zr,Ti)Sb (right part of Figure 8). The bands with dominating $p_\sigma^*$ character occur between 4 and 8 eV above the Fermi level. Note that in the case of (Zr,Ti)Sb, the chain direction corresponds to Γ−Z, which is Γ−Y in the case of the model $^1_\infty[Zr_7Sb_2]$.

The bond order of $^1/_2$ is reflected in a Mulliken overlap population of 0.38 electrons per bond, which is about half of the value expected for a Sb−Sb single bond of 0.65. This compares well to the average values of the corresponding bonds in $(Zr,V)_{13}Sb_{10}$ (0.36) and $(Zr,V)_{11}Sb_8$ (0.34). Comparable values were obtained for longer bonds, namely 0.34 for the shortest Sb−Sb bond (306 pm) in $Zr_2V_6Sb_9$,[19] and 0.26[34] for the Sb−Sb bond in the linear Sb chain (314 pm) in $La_3TiSb_5$,[37] in the case of which simple electron counting leads to an assignment of Sb(−II) and to a bond order of $^1/_2$, also. It is concluded that the mismatch of bond length and strength arises from matrix effects, e.g., because of the equivalency of the lengths of the M4−M4 and Sb4−Sb4 bonds parallel to [001] by symmetry.

**Physical Properties.** The calculations of the electronic structure predict metallic properties for (Zr,Ti)Sb. This is confirmed experimentally. The electrical specific resistivity of $Zr_{0.6}Ti_{0.4}Sb$ increases smoothly from 13 mΩ cm at 10 K to 20 mΩ cm at 290 K, showing the temperature dependence expected for metallic compounds. Grain boundaries might have contributed to the resistivity. However, since the absolute value at room temperature is about $10^4$ times higher than that of copper, a very good metallic conductor, (Zr,Ti)Sb has to be classified as a poorly conducting metal. The Seebeck coefficient of −5.1(1) $\mu$V/K, determined at ambient temperature, is typical for n-type metals, such as sodium (−6.3), niobium (−0.44), or rhenium (−5.9).[38]

## Conclusion

The phase $Zr_{1-x}Ti_xSb$ ($0.38(3) \le x \le 0.549(6)$) was uncovered and subsequently characterized by single-crystal structure analyses, theoretical calculations with the extended Hückel and LMTO approaches, and measurements of the electrical resistivity and thermopower.

Although this phase is situated on the quasibinary section ZrSb−TiSb, its crystal structure is of a new type, and reminiscent only of the TiSb structure, not of ZrSb, and it exhibits structure motifs not found in either ZrSb or TiSb, namely channels formed by M atoms which contain a ladder consisting

(35) Wang, M.; McDonald, R.; Mar, A. *Inorg. Chem.* **1999**, *38*, 3435.
(36) Klinkhammer, K. W.; Pykkö, P. *Inorg. Chem.* **1995**, *34*, 4134.
(37) Bolloré, G.; Ferguson, M. J.; Hushagen, R. W.; Mar, A. *Chem. Mater.* **1995**, *7*, 2229.
(38) Rowe, D. M. *CRC Handbook of Thermoelectrics*; CRC Press: New York, 1995.

of Sb atoms. The latter exhibits strong bonding Sb−Sb interactions (284 pm), which are much shorter than the shortest Sb−Sb distances in ZrSb (324 pm) and TiSb (391 pm).

The metal sites are in part statistically occupied by different mixtures of Zr and Ti atoms, with the smaller Ti atoms preferring the smaller voids in the Sb atom substructure. The differences in the occupancies from site to site decrease with increasing reaction temperature, as the importance of the configurational entropy increases.

The metallic phase (Zr,Ti)Sb is stabilized by heteroatomic M−Sb and (pseudo) homoatomic M−M and Sb−Sb bonds, while the last type of interaction plays only a minor role in ZrSb and is absent in TiSb. However, in all three different structures holes are present in the antimony sp bands, which allow in general the formation of Sb−Sb bonding interactions.

**Acknowledgment.** This work was carried out at the Department of Chemistry of the University of Marburg. Financial support of the Deutsche Forschungsgemeinschaft, the Fonds der Chemischen Industrie, and the Bundesministerium für Bildung, Wissenschaft, Forschung und Technologie is gratefully acknowledged. Insightful discussions with Professor Dr. B. Harbrecht are appreciated.

**Supporting Information Available:** Table of crystallographic data and a thermal ellipsoid figure for (Zr,Ti)Sb and tables of positional and thermal parameters of $Zr_{4.3}Ti_{2.7}Sb_7$, $Zr_{3.7}Ti_{3.3}Sb_7$, and $Zr_{3.2}Ti_{3.8}Sb_7$ (PDF). Three X-ray crystallographic files (CIF). This material is available free of charge via the Internet at http://pubs.acs.org.

JA993423D